Research Article

Tasmia Irshad, Muhammad Saeed, Mamoona Munir, Rehana Kousar, Azeem Intisar*, Muhammad Imran Din, Hadia Ahsan, Muhammad Amin Abid, Muhammad Irfan, and Sameh M. Osman*

Excellent catalytic performance over reduced graphene-boosted novel nanoparticles for oxidative desulfurization of fuel oil

https://doi.org/10.1515/ntrev-2024-0116 received December 5, 2023; accepted October 17, 2024

Abstract: Three new inorganic-organic hybrid nanocomposites (In-WO₃@rGO, Mo-WO₃@rGO, and Mn-WO₄@rGO) were synthesized by hydrothermal method and applied for recoverable and efficacious ODS process of real oil. The physicochemical analysis of novel nanocatalysts was conducted by various techniques, i.e., powder X-ray diffraction, fourier transform infrared spectroscopy, scanning electron microscopy (SEM), energy dispersive X-ray spectroscopy and thermogravimetric analysis. XRD and SEM analyses depicted that the nanoparticles (In-WO₃, Mn-WO₄, and Mo-WO₃) were well embellished on the exterior of reduced GO with an amazing morphology, having a crystallite size of less than 40 nm. The catalytic activity of nanocomposites was scrutinized for real fuel (diesel and kerosene) and model fuel (DBT) using the radical initiator mechanism of the ODS pathway. Excellent efficiency can be obtained under optimized conditions using 0.1 g catalyst, 1 mL oxidant (H_2O_2),

which is lower than that of the other two hybrids. The synthesized nanohybrids showed remarkable durability and recovery up to five times for the ODS process without significant change in proficiency. Keywords: hybrid materials, oxidative desulfurization, model fuel, dibenzothiophene, real fuel

and 100 ppm DBT at 40°C with a time duration of 180 min.

Various factors such as time, DBT concentration, catalyst amount, oxidant amount, and temperature that affect cata-

lytic activity directly or indirectly were also studied. A

pseudo-first-order kinetics model was followed, and due to

spontaneous reaction, a negative value of ΔG was observed

with an activation energy of 6.54 kJ/mol for Mo-WO₃@rGO,

1 Introduction

With the increasing world population, the sulfur content in the atmosphere is increasing day by day because of the emission of gases as a result of excessive human activities such as transportation, electricity, and construction of materials. This increase in sulfur-containing particles causes air pollution and is depleting our environment. The issue of the environment is becoming more severe day by day due to industrialization, urbanization, etc., which are negatively affecting our ecosystem. According to UNO legislation, the limit of sulfur content in HCSs is not to be more than 10 ppm for gasoline and 15 ppm for diesel. Fuel is one of the important sources of energy that is essential for human growth and development. Hence, desulfurization has become one of the worldwide concerns [1,2]. The sulfur contents in fuel are generally classified as disulfides, thiophenes, BT, DBT, mercaptans, etc., which convert sulfur in fuel into SO_x after combustion [3]. In addition, it causes acid rain that contributes to the occurrence of London smog (sulfurous smog), which causes headaches and eye irritation; however, longterm exposure may ultimately cause death. Nowadays, in

e-mail: aa9868591@gmail.com

Tasmia Irshad, Muhammad Saeed, Hadia Ahsan: Centre for Inorganic Chemistry, School of Chemistry, University of the Punjab, Lahore, 54590, **Pakistan**

Mamoona Munir: Department of Botany, Rawalpindi Women University, Rawalpindi, Pakistan

Rehana Kousar: Department of Chemistry, Lahore College for Women University, Lahore, Pakistan

Muhammad Imran Din: Centre for Physical Chemistry, School of Chemistry, University of the Punjab, Lahore, 54590, Pakistan Muhammad Amin Abid: Department of Chemistry, University of Sahiwal, Sahiwal, Pakistan

Muhammad Irfan: Department of Biomedical Physics, Doctoral School of Exact Sciences, Adam Mickiewicz University, Poznan, Poland

^{*} Corresponding author: Azeem Intisar, Centre for Inorganic Chemistry, School of Chemistry, University of the Punjab, Lahore, 54590, Pakistan, e-mail: azeemintisar.chem@pu.edu.pk

^{*} Corresponding author: Sameh M. Osman, Department of Chemistry, King Saud University, Riyadh, Saudi Arabia,

fuel refineries, the main challenge is the removal of sulfur content and its compounds because of strict legislation on environmental remediation [4]. Hydrodesulfurization was the traditional desulfurization technology, which requires hydrogen under high temperature and pressure to eliminate cyclic compounds, i.e., DBT, BT, etc. Therefore, an efficient desulfurization technology needs to be developed that will remove sulfur compounds from fuel to achieve environmental sustainability [5]. Technologies that have been proposed for fuel oil desulfurization, such as adsorptive desulfurization [6], extractive desulfurization [7], bio-desulfurization, and oxidative desulfurization (ODS) [8], are under development [9]. Among all, ODS is gaining colossal attention for the removal of sulfur due to its low cost, higher adaptability for the selectivity of aromatic compounds, high efficiency, and eco-friendly behavior. The scientific community is paying top-tier importance to ODS, as it is the best methodology to liberate sulfurbased ring substances from fluid. This technology requires an oxidative reaction to convert organo-sulfur compounds into sulfones and sulfoxides in the presence of oxidizing agents, such as H₂O₂ under the influence of a suitable catalyst. Then, oxidized compounds are separated by using polar solvents, such as acetonitrile (extractant), through a solvent extraction technique [10]. Over time, this method has evolved into a more beneficial and remarkably cost-effective process, as it now demands microscopic quantities of oxidants and elementary equipment or conditions.

In the past, oxidative catalysis was used in various fields such as water splitting, desulfurization of oil, and pollutant degradation, *etc.* [11]. Desulfurization assisted by ODS is an easily accessible process for the removal of aromatic sulfur compounds from fuel oil owing to mild operating conditions with no consumption of H₂ [12]. ODS is a two-step process: oxidation followed by elimination of sulfones and sulfoxide through extraction using the extractant MeCN. Among the recently used catalysts for ODS, the newly emerging class of modern material POM@MOF-based composites [13], such as supported metal oxides, titanate nanotubes [14], and phase transfer materials, are used as the best choice of catalyst for deep oil desulfurization.

TBA-Si₂W₁₈Mn₄@SAB with CH₃COOH/H₂O₂ as an oxidizing agent was found to be an excellent catalyst for ODS, having 97% removal of sulfur content from gasoline following a first-order reaction. The oxidation reactivity of sulfur compounds is designated in decreasing order as DBT > BT > Th [15]. The nanocomposites for the efficient removal of DBT using Bi₂WO₆@rGo and CuWO₄@rGo catalysts obtained 90% efficiency under optimal reaction conditions via ODS. The kinetics were a pseudo-first-order reaction with optimum energies of 16.91 and 14.57 kJ/mol [16]. (Gly)₃PMo₁₂O₄₀@MnFe₂O₄ hybrid nanocomposites were

used in the CAT-ODS reaction for the withdrawal of dangerous organo-sulfur contents from model fuel oil and gasoline. The removal efficiency was 95% under optimized conditions at a temperature of 35°C with a contact time of 1 h following the kinetics of a pseudo-first-order reaction model. The substrates such as DBT, BT, and Th were catalytically removed with efficiency yields of 98.3, 97.6, and 96.4%, respectively [17]. MOF-derived nanocomposites were used as an efficient catalyst for ODS and ODN.

PTA@H2N-MIL-101-Cr showed excellent efficiency for the removal of DBT from *n*-heptane in the presence of MeCN and H₂O₂ with high reaction rates. Among DBT, 4,6-DMBT, and BT, DBT shows the highest efficiency of 99.6%, followed by 88.2 and 70.5%, respectively [18]. CoW (20)/rGO hybrid nanocomposites were utilized as an efficient catalyst for impressive ODS performance for the model as well as real fuel in the manifestation of hydrogen peroxide [19]. Recent studies show that the rGO-based catalyst for the removal of sulfur compounds effectively contributes to cleaner energy production and a safer environment. Moreover, the importance of hybrid Ni/Fe₃O₄/rGO is its large surface area and electrical conductivity that facilitate the effective adsorption and activation of sulfurcontaining compounds [20]. This catalyst showed excellent sulfur removal efficiency in model diesel fuel, surpassing traditional catalysts in terms of activity and durability. Another heterogeneous catalyst, FeW₁₁V@CTAB-MMT, used for ODS of gasoline following pseudo-first-order kinetics, has the best removal efficiency of DBT, BT, and Th with more than 97% efficiency at 35°C after 1 h [21]. This catalyst is perfectly used to remove hazardous sulfur compounds from gasoline. Homogeneous and heterogeneous polyoxometalates are used as efficient catalysts for the ODS process of fuel by removing refractory sulfur compounds, e.g., DBT and BT, under mild reaction conditions but with high efficacy [22]. The heterogeneous catalyst $Fe_6W_{18}O_{70} \subset CuFe_2O_4$ exhibited an extraordinarily high efficiency with the removal of thiophene 98%, DBT 99%, and BT 99% when used in ultra-deep ODS of real gasoline and simulated fuel. The reaction occurs under optimized conditions of a temperature of 35°C with a contact time of 1 h and shows an oxidation reaction efficiency of 95% [23].

In recent years, carbon materials, particularly graphene oxide, have been utilized as catalyst support for ODS because of their special surface properties, unique interlayer structure, and extremely large surface area. Reduced graphene oxide (rGO) is a two-dimensional, crystalline allotrope possessing a six-membered ring, lattice structure made from pure carbon atom, sp² hybridization, with unique electrical and thermal properties [24]. A high surface area results in more active sites for the catalytic

reaction, allowing effective adsorption of sulfur-containing compounds. While rGO-based nanocomposites play a vital function in this process, immense research concerning the ODS of oil by hybrid materials needs to be paid attention to. Researchers have reported rGO-supported TM-modified catalysts, mesoporous silica, and MOF@POM hybrid materials for efficient and green ODS. 2D-GO not only possesses great thermal and electrical properties but also contains functional groups having oxygen that play an essential role in chemical modifications. These hybrid nanocomposites have found applications in diverse fields of interest, playing a decisive role in advancing modernization breakthroughs and facilitating innovation in the realms of energy and environment. As a result, their utilization spans various sectors within these environmental domains [24]. Moreover, owing to rGO, chemical stability is enhanced, ensures long-term stability of catalysts, and reduces operational cost.

The current work includes fabrication of Mo–WO₃@rGO, Mn–WO₄@rGO, and In–WO₃@rGO nanocomposites (recoverable, TM-free) and their catalytic testing for the ODS process for oils. The characterization of the prepared materials is performed using scanning electron microscopy (SEM), XRD (powder X-ray diffractometer), energy dispersive X-ray spectroscopy (EDX), IR spectroscopy, and thermogravimetric analysis (TGA) study. Various parameters, including the concentration of sulfur content, time interval of absorption–desorption equilibrium, temperature, and catalyst concentration, were investigated to regulate the ODS process. Furthermore, the recovery of the catalyst, mechanism and testing of oil were inspected, and detailed insights into these aspects are provided in the subsequent analysis.

2 Materials and methods

2.1 Materials

KMnO₄ 99.9%, H_2SO_4 98%, graphite powder, H_2O_2 30% by weight, prepared catalysts (In–WO₃@rGO, Mn–WO₄@rGO, and Mo–WO₃@rGO), hydrochloric acid (HCl, 37%), Na₂WO₄·2H₂O 99%, and dibenzothiophene (DBT) were purchased from Sigma-Aldrich Co., and indium sulfate [In₂(SO₄)₃], manganese acetate $C_4H_{14}MnO_8$, and ammonium molybdate 4-hydrate [(NH₄)₃ Mo₇O₂₄·4H₂O] were acquired from Merck.

2.2 Production of GO, exfoliated GO, and reduced GO

rGO was prepared following an earlier method with a few minor modifications [24]. An ice bath was used for half an hour to maintain the temperature <5°C while mixing continuously, and 4 g of powdered graphite was weighed and placed in a beaker with 100 mL of pure sulfuric acid. The main purpose of using an ice bath was to maintain temperature to avoid thermal degradation of the GO precursor material, as high temperature may lead to incomplete synthesis or degradation of the desired product. Thus, cooling the reaction media helps to obtain better control of reaction conditions. The mixture was constantly stirred after introducing 12 g of KMnO₄ while keeping the temperature below 10°C in a cold pot. Later, it was diluted by the addition of 100 mL of deionized H₂O with constant shaking. H₂O₂ (30 wt%) was added to the mixture to reduce the remaining KMnO₄. Then, screening was completed, the deposit was separated by filtration, and it was rinsed with 5% aqueous solution of HCl and water till the pH remained 6 to further guarantee that ions were eradicated. Hydrogen peroxide played a vital role as an oxidizing agent, often used to oxidize graphene to GO by initiating oxygen-containing groups, i.e., hydroxyl groups, epoxide to the graphene sheet, and transforming sp² carbon atoms to sp³ hybrid form. Dehydration of the GO product was carried out at 45°C for 1 day in a furnace.

Exfoliation of the product was performed by dissolution of 2 g of GO in 500 mL of deionized water with constant stirring for 6 h. As unexfoliated nanocomposite piped out during the reaction, the synthesized XGO was then dehydrated for a day at 45°C, and centrifugation and ultrasonication were performed to remove any unexfoliated GO. XGO (1g) was introduced to 0.5 L of distilled water to synthesize rGO by heating and stirring at 90°C for 4 days. The prepared rGO at 120°C was dried in an oven.

2.3 Synthesis of In–WO $_3$, Mn–WO $_4$, and Mo–WO $_3$, In–WO $_3$ @rGO, Mn–WO $_4$ @rGO, and Mo–WO $_3$ @rGO

For the preparation of $In-WO_3$, 1g of Na_2WO_4 and 1g of $In_2(SO_4)_3$ were mixed in a 250 mL beaker containing 100 mL of deionized water. The mixture was stirred for 25–30 min. After agitation, sodium borohydride (NaBH₄) was added to the beaker containing the previous mixture till the formation of bubbles stopped. Later, it was placed in a Teflonassisted steam vessel/cylinder and kept in a furnace for 6 h at 155°C. The same procedure was adopted for $Mn-WO_4$ and $Mo-WO_3$ using manganese and molybdenum salts, *i.e.*, manganese acetate and ammonium molybdate, respectively. A combination of TMs (indium, manganese, and molybdenum) supported on rGO was created by

incorporating ~20% TMs-WO $_3$ onto ~80% rGO. The fabrication was done using an autoclave at 150°C for 7–8 h. These parameters of time and temperature conditioning are very crucial as this temperature range allows the uniformity of composite structures and also increases the diffusion of the precursor. Moreover, all MOs required a specific range of optimal temperatures for the synthesis of the desired hybrid oxides. In addition, the duration of the autoclave gives the overall reaction time and extent of interaction between rGO sheets and TMs-WO $_3$. These two factors depict the overall morphology, phase composition, and crystallinity of nanohybrids, and their adjustments control the synthesis mechanism. After filtration, the products (In–WO $_3$ @rGO, Mn–WO $_4$ @rGO, and Mo–WO $_3$ @rGO) were heated for 6 h at 300°C.

2.4 Characterization techniques

The prepared materials (In–WO₃@rGO, Mn–WO₄@rGO, and Mo–WO₃@rGO) were subjected to characterization using multiple techniques, such as FT-IR spectroscopy using IR-TRACER-100, a wavelength of 4,000–400/cm with a scanning speed of 15/cm; powder X-ray diffraction of Cu-k α (0.154 nm or 1.54 Å) with a range of 5°–70° and a scanning speed of 2°/min; SEM for morphology was performed using NOVA NANO together with EDX and TGA under an inert atmosphere in the range of 400–800°C. Furthermore, the properties of fuel were assessed using PETRA-XRF, a total sulfur tester ASTM D-4294, an H₂O content analyzer (China PT-D4006-8929A, volume %, ASTM D-4006), a hydrometer (density analyzer) at 15.6°C @gmol⁻¹, ASTM D-1298), and a Distillation Tester (ASTM D-86, PAC, PMD 110).

2.5 ODS procedure

Catalytic testing was inspected using 1,000 ppm DBT in n-hexane and 40 mL of an extractant using 0.1 g of the catalyst (In–WO₃@rGO, Mn–WO₄@rGO, and Mo–WO₃@rGO) under ideal conditions, and the conditions for the catalytic reaction were optimized to achieve the best possible performance. The mixture (model fuel, extractant, and catalyst) was poured into a cone-shaped flask and kept in the absence of light for 15 min to obtain as adsorption–desorption stability curve. Later on, 1 mL of 30 wt% oxidant H_2O_2 was added to the flask. The reaction converts sulfur compounds in model fuel to sulfones. Then, sulfoxides were liberated in a polar medium containing extractants; thus, other rested sulfur in the non-polar medium can be calculated using an ultravioletvisible spectrometer with λ_{max} = 285 nm (transition from n to

 $\pi^*).$ Moreover, a total sulfur analyzer (PETRA XRF) was utilized to measure the amount of rested sulfur in the liquid phase at various time spans. The effectiveness of model fuel elimination could be determined using the mathematical equation:

Desulfurization (%) =
$$C_i - C_f/C_i \times 100$$
.

Here, C_f is the final amount of DBT in model fuel, and C_i is the original amount of DBT in the fuel determined by ultraviolet-visible spectroscopy.

3 Results and discussion

3.1 Characterization

3.1.1 FT-IR spectroscopy

FT-IR spectroscopy is majorly concerned with the vibration of molecules that correspond to specific vibrational energy levels. FT-IR studies were performed to investigate the vibrational band stretching of functional groups present in the prepared rGO and its hybrid materials, Mo-WO3@rGO, Mn-WO4@rGO, and In-WO₃@rGO in the range between 4,000 and 400/cm, as shown in Figure 1. In rGO, the characteristic peaks were observed: 3,600–3,200/cm (–OH stretching), 3,050/cm (sp² CH stretching), 2,915/cm (sp³ CH stretching), 1,730/cm (C=O stretching), 1,600-1,500/cm (C=C stretching of aromatic ring), 1,200-1,100/cm (C-O stretching), and 1,030/cm (C-C stretching), all these crests are the clear verification of the formation of rGO material successfully. All the peaks are similar in rGO-supported nanocomposites with just one extra peak owing to the M-O bond peak at 600-500/cm (M = W), which confirms the formation of composites fruitfully.

3.1.2 XRD

X-ray diffraction of Cu-k α (0.154 nm) with a span of 2θ = 5°-70° was used to verify the XRD spectrum of rGO and In-WO₃@rGO, Mn-WO₄@rGO, and Mo-WO₃@rGO to measure the average crystallite size, basal plane, and crystal system, as shown in Figure 2. There is just a single characteristic peak in the XRD spectra of rGO at 2θ = 26.3° having a basal plane of the (002) plane with a *d*-space of 0.34 nm, consistent with the *JCPDS* Card No. 75-2078. The (002) plane, ascribed to the lighter films of rGO due to greater extent of flaking as well as phase of rGO, is quite comparable to g-C₃N₄. It is confirmed that graphitic coatings may be diminished after loading with nanocomposites

DE GRUYTER Oxidative desulfurization of fuel oil — 5

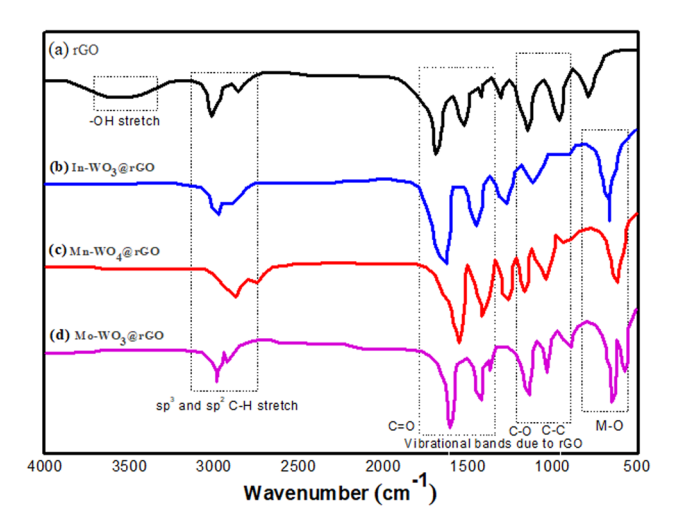


Figure 1: IR vibrational analysis of (a) rGO, (b) In-WO₃@rGO, (c) Mn-WO₄@rGO, and (d) Mo-WO₃@rGO.

of In–WO₃@rGO, Mn–WO₄@rGO, and Mo–WO₃@rGO that leads to stacking in an irregular pattern when the intensity of the peak with a basal plane of (002) decreased. Graphene strips are separated into thinner layers with varying latticework, differentiating them from both GO and graphite flakes, as documented in earlier studies. The notable peaks in nanoparticles are as follows: In–WO₃@rGO: 2θ = 20.1 (020), 31.5 (222), 63.47 (622); Mn–WO₄@rGO: 2θ = 20.23 (100), 32.73 (111), 35.81 (002), 45.21 (211), 62.01 (113); and Mo–WO₃@rGO: 2θ = 17.37 (110), 27.81 (300), 34.21 (310), 49.37 (002), 52.32 (211), in which (002), (222), and (020) are correlated with WO₃ (JCPDS card no.

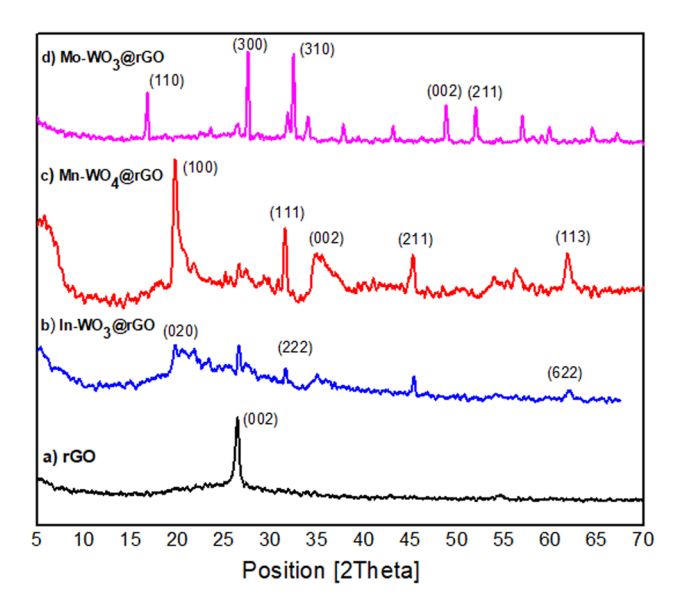


Figure 2: XRD pattern of (a) rGO, (b) In-WO $_3$ @rGO, (c) Mn-WO $_4$ @rGO, and (d) Mo-WO $_3$ @rGO.

72-1465) [25]. As indicated by JCPDS card no. 72-1465, pure WO₄ demonstrates the monoclinic crystal structure as outlined in the previous literature, and after successful loading of In and Mo into WO₃ makes an orthorhombic geometry. In the XRD pattern of Mn–WO₄@rGO, (100), (111), and (113) planes are due to the presence of Mn. Moreover, impurity related peaks have not been found in hybrid materials that depicted the loading of M onto the W latticework rather than the interstitial sites [19]. The average crystallite size was determined through the Debye–Scherrer equation $(D = (k\lambda)/(\beta \cos \theta))$, where Scherrer constant (k) is equal to 0.9, λ is the wavelength of Cu-ka (0.154 nm), β is the full width at half-maximum, and θ is the Bragg's angle. The mean crystallite size of rGO, In-WO₃@rGO, Mn-WO₄@rGO, and Mo-WO₃@rGO are 18.78, 37.66, 23.41 and 21.26 nm, respectively. Notably, the intensity of the rGO peak is lowered in composites due to doping effect, structural changes, inference, and interaction with other materials in the composites. Composites have diffraction peaks that overlap with rGO peaks, making it hard to distinguish them separately.

3.1.3 SEM and EDX

SEM uses an intensive beam of energized electrons, instead of light, that investigates the morphology and chemical composition for imaging by scanning and normally for micrometer or nanometer particulates. The micrographs of rGO (Figure 3(a)) and rGO-supported novel nanocomposites of In-WO₃@rGO (Figure 3(b) and (c)), Mn-WO₄@rGO (Figure 3(d) and (e)), and Mo-WO₃@rGO (Figure 3(f) and (g)) were collected using a NOVA NANO SEM. The results revealed that rGO is primarily composed of wrinkled, thin, overlapped sheets, and agglomerated solids were placed willy-nilly with precise and well-defined edges [26]. The indefinite rGO sheets exemplify a clear and apparent manifestation of GO flaking as the length between sheets reduced; however, in composites of rGO, due to doping phenomena, random particles were visible on the exterior of rGO [27]. At elevated magnification, an even dispersion on the exterior of rGO in the case of nanocomposites confirms that rGO granules are not single, but some of them are accumulated between overlapped and agglomerated rGO sheets [28,29]. The particles of In, Mn and Mo are decorated very well on the surface of the rGO sheets and showed interesting morphology, which increased its catalytic activity by increasing the surface area and change in morphology. Furthermore, EDX analysis was used to explore the component pattern in rGO-based materials with X-rays. The occupancy of In, Mn, Mo, and W together with carbon and oxygen atom vertex confirm that In-WO3, Mn-WO4, and

6 — Tasmia Irshad et al. DE GRUYTER

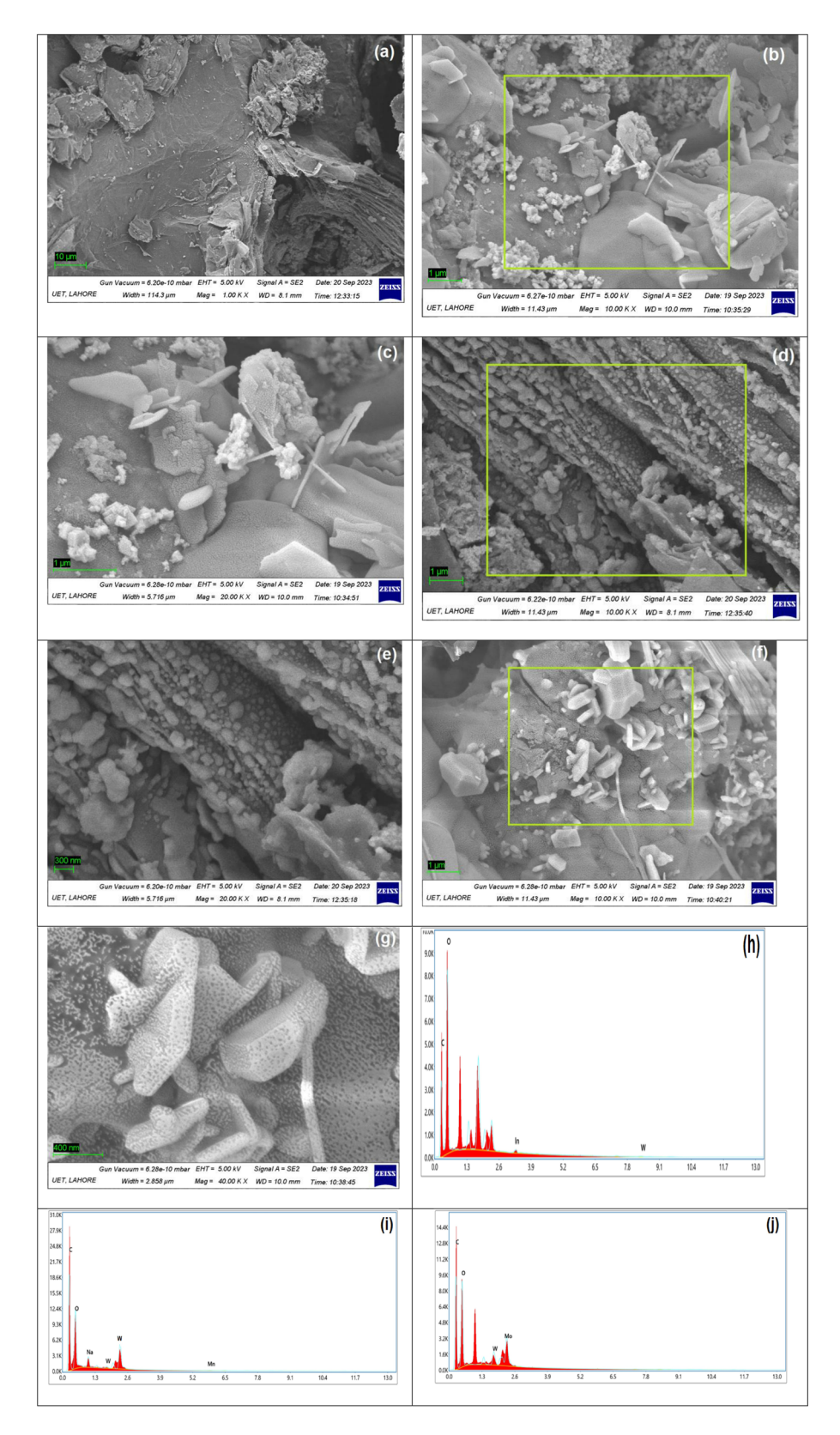


Figure 3: SEM micrographs of rGO (a), In-WO₃@rGO (b) and (c), Mn-WO₄@rGO (d) and (e), and Mo-WO₃@rGO (f) and (g). EDX of In-WO₃@rGO (h), Mn-WO₄@rGO (i), and Mo-WO₃@rGO (j).

 $Mo-WO_3$ are successfully doped onto rGO (Figure 3(h), (i) and (j)).

3.1.4 TGA

TGA was performed to observe the heat endurance and disintegration activity of the synthesized materials in the range of 40-800°C, with a scan rate of 5°C/min under inert (He) environments. As shown in Figure 4, at 100-150°C, due to the vaporization of water molecules or other impurities present in rGO, a slight mass loss of 20% was observed [30]. However, for composites (In-WO₃@rGO, Mn-WO₄@rGO, and Mo-WO3@rGO), only 9% weight loss was observed up to 200°C, which depicts the loss of remaining oxygen molecules and removal of water molecules that are connected with the surface of rGO. Next, in the range of 300-450°C, 49% mass loss is associated with the removal of carbonaceous material for composites (In-WO₃@rGO, Mn-WO₄@rGO, and Mo-WO₃@rGO). After 550°C, no significant weight loss was observed for composites and unchangeable mass is reduced to 800°C. Moreover, up to 800°C, almost 80-85% decomposition of rGO took place, which confirmed that temperature had a remarkable effect on the thermal properties of the composites. Pure rGO has a greater weight loss compared to composites in the range of 500-700°C, which proves that nanocomposites are more efficient and reliable for catalytic activity. The hardness, modulus of elasticity, yield strength, and durability of alloy and metal increased as the temperature decreased. In addition, the composites (In-WO3@rGO,

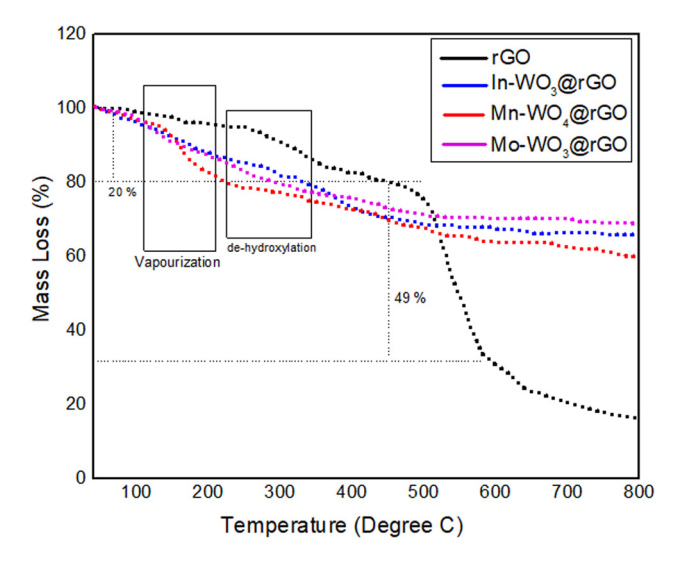


Figure 4: TGA weight loss curves of rGO, In-WO₃@rGO, Mn-WO₄@rGO, and Mo-WO₃@rGO.

Mn–WO₄@rGO, and Mo–WO₃@rGO) show significant affinity and high thermal stability with rGO.

All characterization techniques complement each other by giving in-depth information about the structure of the material, properties, composition, and nature of the composite. IR spectroscopy gives an in-depth understanding of the functional group identification that helps us to correlate the crystallinity determined by XRD. SEM informs about the shape, particle size, and surface topography, while EDX confirms the composition of specific regions identified in SEM images. Overall, all these allow researchers to know about materials' potential, synthesis, optimization, quality control, and applications.

3.2 Optimization

Experiments at different temperatures and times were conducted to determine the effect of temperature (25, 45, 60, and 90°C) and time (30, 60, 90, 120, and 180 min), where other parameters were kept constant such as the catalyst, DBT concentration, and amount of H₂O₂. Illustrating from the graph (temperature versus efficacy), it is unambiguous that temperature had an inverse effect on the activity of the catalyst, which means an increase in temperature decreases the catalytic activity [31]. However, in the case of the time vs efficiency plot, time is directly related to the activity of the stimulant [32]. This is evident that with an increase in temperature, the activity of the catalyst and reaction rate decrease due to the decomposition of the oxidant, as shown in Figure 5(a) and (b). Hence, optimized parameters of time of 2h and temperature of 45°C were used for subsequent study.

Regarding the effect of DBT amount, as shown in Figure 5(c) (50, 100, 200, and 500 mg/L), it is clear that it has an indirect effect with efficiency as a constant catalyst dose is insufficient to provide catalytic sites to oxidize 500 mg/L in 2 h. Hence, a prolonged duration is recommended to oxidize sulfur containing compounds thoroughly at high concentrations. It was investigated that if lower the dose of DBT molecules, the more effective the desulfurization under optimized conditions. As the catalyst amount has foremost effect on catalytic effectiveness, as shown in Figure 5(d), it is clearly investigated that the stimulant dose effects on efficacy (0.05-0.2 g of In-WO₃@rGO, Mn-WO₄@rGO, and Mo-WO₃@rGO) has positive effect on the catalytic activity while keeping other parameters constant, i.e., the time interval, temperature, DBT extent, and quantity of oxidant. The efficiency of materials (In-WO₃@rGO, Mn-WO₄@rGO, and Mo-WO₃@rGO) enhanced to 99.8% when the catalyst amount increased from 0.05 to 0.2 g. A greater amount of

8 — Tasmia Irshad et al. DE GRUYTER

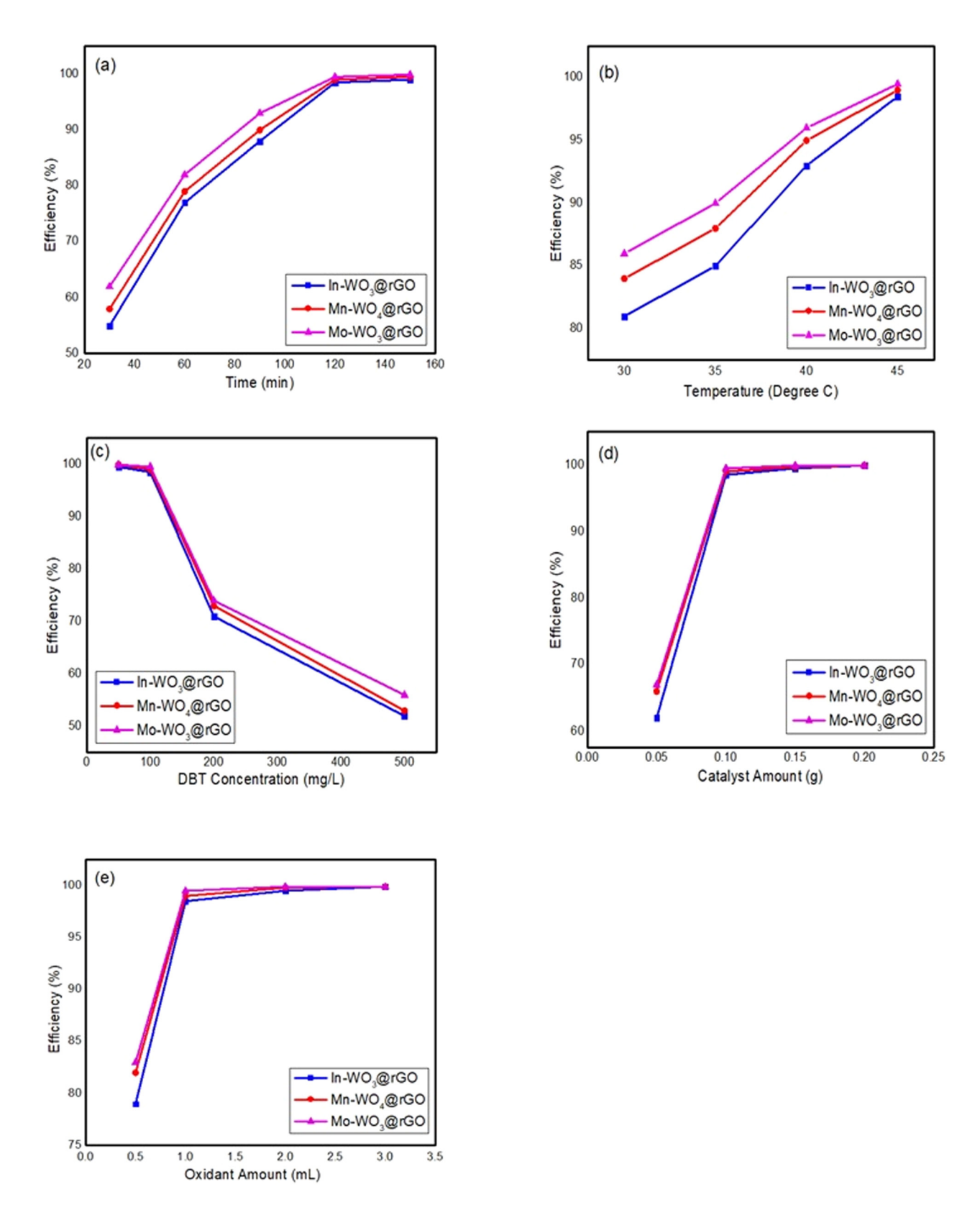


Figure 5: Impact of time (a), temperature (b), DBT dose (c), catalyst amount (d) and oxidant amount (e) on desulfurization of DBT.

DBT remained unoxidized due to a small dose of catalyst, as there were few catalytic sites available to perform the reaction [33]. Moreover, further increase in the catalyst dosage decreased the catalyst efficiency due to catalyst agglomeration, which blocked the active sites. It is clear from the figure that greater efficiency was achieved by Mo-WO3@rGO compared to the other TMs-WO₃ hybrids (Mn-WO₄@rGO and In-WO₃@rGO), and the highest DBT conversion through Mo-WO3@rGO because of changes in auxiliary/secondary metal performance from regulator to opponent and excellent metal-supported interactions. Moreover, TM molybdenum (Mo)-based hybrid material have low adsorption energy, which results ultimately in lower Ea compared to manganese (Mn) and indium (In). Hydrogen peroxide, which is an oxidant, has a main role in the desulfurization of DBT as it was used as an initiator in reaction media. By maintaining other parameters steady (0.1 g catalyst, 100 mg/L DBT model fuel, 45°C, and time 120 min), the amount of oxidant was changed (0.5, 1.0, 2.0, and 3.0 mL) to determine the effect of the oxidant on the efficacy, as depicted in Figure 5(e). Concluding the optimized conditions, a greater quantity of catalyst will lower the DBT content (1 mL of oxidant at approximately 40-45°C), as high concentrations of catalyst may raise the probability of maximum oxidation of sulfur content in the fuel. The study clearly investigated that the H₂O₂ oxidant has a positive impact on efficiency as it expedites by increasing the amount of initiator/ oxidant. Further, no effect was observed when the amount exceeds 2 mL. In this reaction medium, H₂O₂ acts as an initiator, which confirms its positive behavior by depicting that with the increase in the promoter amount, the efficiency of the catalyst also increases. In the ODS process, hydrogen peroxide as an oxidizing agent has the potential to selectively oxidize sulfur and sulfur-containing compounds (lower oxidation state) under ambient conditions of pressure and temperature and convert them into polar compounds of sulfones and sulfoxides (higher oxidation states).

3.3 Kinetics, thermodynamics, and the ODS mechanism

Kinetic studies provided strong evidence in support of speed and oxidative processes, as they follow the pseudo-firstorder kinetic model. From this, the value of the constant is measured, which helps in the estimation of the kinetics of the oxidation reaction [34]. A plot of C_F/C_I versus time (min) at various temperatures is demonstrated only for Mo–WO₃@rGO, as it showed the highest efficiency compared to In–WO₃@rGO and Mn–WO₄@rGO (Figure S1) and the coherence coefficient (R^2) was ~1, where C_I is the initial concentration and C_F is the final concentration of the DBT solution, indicating that the ODS reaction followed pseudo-first-order kinetics at temperatures of 30, 35, 40 and 45°C. Moreover, the optimum energy in the ODS process of DBT can be estimated via the Arrhenius plot by drafting coordinates $ln\ K\ vs\ 1/T$. The values are calculated using the Arrhenius equation and it was 6.540 kJ/mol for Mo–WO₃@rGO. The Arrhenius equation is given as

$$K = Ae^{-Ea/RT}$$
.

To understand the effect of temperature on DBT oxidation, a curve was plotted between $\ln K_c$ and 1/RT to calculate the standard Gibbs free energy (ΔG), enthalpy of activation (ΔH°), and entropy of activation (ΔS) *via* the Eyring equation [35]

$$\ln K_{\rm c} = \frac{-\Delta H}{RT} + \frac{\Delta S}{R}.$$

In this equation, T denotes absolute temperature, K and K_c denotes equilibrium constant where ΔG (the standard Gibbs free energy) can be evaluated using [36,37]

$$\Delta G = -RT \ln K_c$$

From the plot $\ln K_c vs 1/RT$, the given outcomes show positive values of ΔS and ΔH depicting an endothermic process and haphazardness in the reaction medium, respectively, as listed in Table 1. However, negative values of the standard Gibbs free energy indicate that DBT removal via In–WO₃@rGO, Mn–WO₄@rGO, and Mo–WO₃@rGO is a stable and thermodynamically useful ODS process.

3.4 ODS of real fuel oils

Catalytic testing of synthesized nano-composites (In–WO₃@rGO, Mn–WO₄@rGO, and Mo–WO₃@rGO) was carried out for fuel samples available in the market using 0.2 g catalyst, 3 mL of $\rm H_2O_2$, 50 mL of fuel sample, and time span of 180 min at 45°C.

Table 1: Thermodynamic factors affecting the removal of sulfur content (DBT) through oxidative desulfurization

Novel catalyst		Δ <i>G</i> (k	ΔH (kJ/mol)	ΔS (kJ/mol K)		
	298.5 K	303.5 K	308.5 K	313.5 K		
Mo−WO₃@rGO	-0.506	-2.551	-5.193	-14.016	260.27	0.854

Table 2: ODS of real oil via In-WO₃@rGO, Mn-WO₄@rGO and Mo-WO₃@rGO

Fuel and catalysts			Specific gravity	Total sulfur by petra	Water content	Distillation (°C)	
		(g/mL at 15.6°C)	X-ray (ppm)	(vol%)	50%	90%	
Kerosene	Before ODS		0.831	1,525	Nil	241	304
	After ODS	In−WO₃@rGO	0.830	135	Nil	236	302
		Mn-WO ₄ @rGO	0.828	144	Nil	238	299
		Mo−WO₃@rGO	0.827	152	Nil	238	298
Diesel	Before ODS		0.885	4,596	Nil	286	345
	After ODS	In-WO₃@rGO	0.882	425	Nil	279	337
		Mn-WO ₄ @rGO	0.879	433	Nil	279	342
		Mo−WO₃@rGO	0.877	449	Nil	280	338

To determine the sulfur content, pre- and post-ODS processes were completed *via* PETRA XRF. Moreover, other fuel properties such as distillation (ASTM D-86), moisture content (ASTM D-4006), and relative gravity (ASTM D-1298) were also investigated before and after ODS and provided in Table 2. A slight difference was noted before and after ODS in fuel properties, which is a clear confirmation that the catalytic system does not impact the characteristics of oil except specific elimination of sulfur species [38,39]. From the ODS of oil (In–WO₃@rGO, Mn–WO₄@rGO, and Mo–WO₃@rGO), results declared that Mo–WO₃@rGO is slightly more efficient than In–WO₃@rGO and Mn–WO₄@rGO for both real and model fuel. Besides this, all nanocomposites proved optimistic and robust for the effective removal of DBT.

3.5 Reusability of catalyst

Catalysts speed up the reaction mechanism, depriving of a structural or compositional modification, *i.e.*, help to cause

a reaction at a faster rate by reducing the activation energy of the chemical reaction. The reusability of the catalyst plays an important role due to its practical uses as it assesses the financial viability of the newly created catalyst scheme. To test restoration and recovery of catalysts (Mo-WO₃@rGO, Mn-WO₄@rGO, and In-WO₃@rGO) via simple filtration technique, first, it is detached from the reaction medium, rinsed with *n*-hexane/dichloromethane (any non-polar solvents), dried, and reused. After the evaluation test of reusability was performed, results indicated no significant alteration in the efficacy of the catalyst for the conversion rate of DBT even after five times. A slight loss in efficiency was noted after five cycles, and this occurred due to a decrease in catalytic sites and mass damage of the catalyst during the purification process. The catalysts (Mo-WO₃@rGO, Mn-WO₄@rGO, and In-WO3@rGO) showed excellent stability and maintained its potency up to five catalytic rounds. Previously reported studies for ODS using rGO-based catalysts are provided in Table 3. The reported literature confirmed that there is no report on rGO as supported TMs (Mo, Mn, and In) doped

Table 3: Comparison with other reported studies

Material	Oxidant	Sulfur specie	DBT concentration (ppm)	Efficiency (%)	References
Bi ₂ WO ₆ @rGO	H_2O_2	DBT	100	97	[16]
CuWO ₄ @rGO		DBT	100	99	
NiWO ₃ @g-C ₃ N ₄	H_2O_2	DBT	100	97	[2]
		Kerosene	1,635	91.5	
		Diesel	4,630	89.5	
$WO_3/g-C_3N_4$	H_2O_2	DBT	500	91.2	[40]
NiW/rGO	H_2O_2	DBT	500	>90	[19]
CoW/rGO	H_2O_2	DBT	500	~100	
CoMo/rGO	H_2O_2	DBT	500	99	[41]
g-C ₃ N ₄	TBHP	DBT	500	>10	[42]
$MoO_2/g-C_3N_4$	TBHP	DBT	500	~100	
Mo-WO ₃ @rGO	H_2O_2	DBT	500	99.8	Current study
Mn-WO ₄ @rGO	H_2O_2	DBT	500	99.5	Current study
In−WO₃@rGO	H_2O_2	DBT	500	99	Current study

tungstate. This study consisting of newly synthesized hybrids of Mo–WO₃@rGO, Mn–WO₄@rGO, and In–WO₃@rGO have been certified for the first time for the oxidative process for the extraction of DBT. Moreover, there are sufficient reported data on rGO-assisted transition metal-based catalysts.

4 Conclusion

The fruitful hydrothermal treatment of rGO-supported nanohybrids was carried out for the first time for ODS of real as well as model fuel. Out of these three hybrids, remarkable desulfurization efficiency of model fuel was accompanied by Mo-WO₃@rGO 98.5% using H₂O₂ as an oxidant. XRD results revealed an average crystallite size of less than 40 nm, and morphology observed through SEM indicated that hybrids are well embellished on the exterior of rGO. The activity for real fuel oil was scrutinized by using these three catalyst and removal efficiencies were 90.23 and 90.03% for diesel and kerosene oil for In-WO₃@rGO; for Mo-WO₃@rGO, 90.7 and 91.15%; for Mn-WO₄@rGO, 90.57 and 90.55%, respectively, under optimum conditions. Multiple parameters such as time, catalyst amount, oxidant amount, and concentration were determined and found that all had a direct relationship with efficiency, except the DBT concentration that followed a pseudo-first order with a negative value of ΔG , depicting thermodynamic stability at 298.5, 303.5, 308.5, and 313.5 K. In addition, five times reusability of the catalyst confirmed its stability, with little reduction in effectiveness for the ODS process. Therefore, complete novel innovation depicts the eminence of the synthesized nanomaterials for the green generation of sulfur-free fluid.

Acknowledgments: The authors are grateful to the University of the Punjab for assistance.

Funding information: The authors state no funding involved.

Author contributions: All authors have accepted responsibility for the entire content of this manuscript and approved its submission.

Conflict of interest: The authors state no conflict of interest.

Data availability statement: Data sharing is not applicable to this article as no datasets were generated or analyzed during the current study.

References

- [1] Jabar G, Saeed M, Khoso S, Zafar A, Saggu JI, Waseem A. Development of graphitic carbon nitride supported novel nanocomposites for green and efficient oxidative desulfurization of fuel oil. Nanomater Nanotechnol. 2022:12:1–13.
- [2] Saeed M, Munir M, Intisar A, Waseem A. Facile synthesis of a Novel Ni-WO₃@g-C₃N₄ nanocomposite for efficient oxidative desulfurization of both model and real fuel. ACS Omega. 2022;7:15809–20.
- [3] Ahsan H, Anayyat U, Saeed M, Anwar A, Haider S, Intisar A, et al. Synthesis, characterization and catalytic activity of rGO supported novel hybrid materials for green fuel production. J Indian Chem Soc. 2024;101:101141.
- [4] Lu L, Cheng S, Gao J, Gao G, He MY. Deep oxidative desulfurization of fuels catalyzed by ionic liquid in the presence of H₂O₂. Energy Fuels. 2007;21:383–4.
- [5] Rivoira LP, Valles VA, Martínez ML, Sa-ngasaeng Y, Jongpatiwut S, Beltramone AR. Catalytic oxidation of sulfur compounds over Ce-SBA-15 and Ce-Zr-SBA-15. Catal Today. 2021;360:116–28.
- [6] Saeed M, Riaz A, Intisar A, Iqbal Zafar M, Fatima H, Howari H, et al. Synthesis, characterization and application of organoclays for adsorptive desulfurization of fuel oil. Sci Rep. 2022;12:7362.
- [7] Rezvani MA, Ardeshiri HH, Aghasadeghi Z. Extractive-oxidative desulfurization of real and model gasoline using (gly)₃H[SiW₁₂O₄₀] ⊂ CoFe₂O₄ as a recoverable and efficient nanocatalyst. Energy Fuels. 2023;37:2245–54.
- [8] Saeed M, Waseem A, Intisar A. Catalytic activity of MnWO₄@g-C₃N₄ and CuWO₄@g-C₃N₄ nano-composites for green fuel production. Catal Surv Asia. 2024. doi: 10.1007/s10563-024-09437-y.
- [9] Haruna A, Merican ZMA, Musa SG. Recent advances in catalytic oxidative desulfurization of fuel oil – A review. J Ind Eng Chem. 2022;112:20–36.
- [10] Hossain MN, Park HC, Choi HS. A comprehensive review on catalytic oxidative desulfurization of liquid fuel oil. Catalysts. 2019;9:229.
- [11] Jiang W, Zhu W, Chang Y, Chao Y, Yin S, Liu H, et al. Ionic liquid extraction and catalytic oxidative desulfurization of fuels using dialkylpiperidinium tetrachloroferrates catalysts. Chem Eng J. 2014;250:48–54.
- [12] Chen L, Ren JT, Wang HY, Sun ML, Yuan ZY. Engineering a local hydrophilic environment in fuel oil for efficient oxidative desulfurization with minimum H₂O₂ oxidant. ACS Catal. 2023;131:2125–33.
- [13] Rezvani MA, Shaterian M, Akbarzadeh F, Khandan S. Deep oxidative desulfurization of gasoline induced by PMoCu@MgCu₂O₄-PVA composite as a high-performance heterogeneous nanocatalyst. Chem Eng J. 2018;333:537–44.
- [14] Lorençon E, Alves DCB, Krambrock K, Ávila ES, Resende RR, Ferlauto AS, et al. Oxidative desulfurization of dibenzothiophene over titanate nanotubes. Fuel. 2014;132:53–61.
- [15] Rezvani MA, Aghbolagh ZS, Monfared HH. Green and efficient organic-inorganic hybrid nanocatalyst for oxidative desulfurization of gasoline. Appl Organomet Chem. 2018;32:e4592.
- [16] Riaz A, Saeed M, Munir M, Intisar A, Haider S, Tariq S, et al. Development of reduced graphene oxide-supported novel hybrid nanomaterials (Bi₂WO₆@rGO and Cu-WO₄@rGO) for green and efficient oxidative desulfurization of model fuel oil for environmental depollution. Environ Res. 2022;212:113160.

- [17] Rezvani MA, Khandan S, Rahim M. Synthesis of (Gly)₃PMo₁₂O₄₀@MnFe₂O₄ organic/inorganic hybrid nanocomposite as an efficient and magnetically recoverable catalyst for oxidative desulfurization of liquid fuels. Int J Energy Res. 2022;46:2617–32.
- [18] Bhadra BN, Jhung SH. Oxidative desulfurization and denitrogenation of fuels using metal-organic framework-based/-derived catalysts. Appl Catal, B. 2019;259:118021.
- [19] Hasannia S, Kazemeini M, Seif A, Rashidi A. Oxidative desulfurization of a model liquid fuel over an rGO-supported transition metal modified WO₃ catalyst: Experimental and theoretical studies. Sep, Purif Technol. 2021;269:118729.
- [20] Rashid T, Raza A, Saleh HAM, Khan S, Rahaman S, Pandey K, et al. Green synthesis of Ni/Fe3O4/rGO nanocomposites for desulfurization of fuel. ACS Appl Nano Mater. 2023;6:18905–17.
- [21] Rezvani MA, Khandan S. Synthesis and characterization of a new nanocomposite (FeW₁₁V@CTAB-MMT) as an efficient heterogeneous catalyst for oxidative desulfurization of gasoline. Appl Organomet Chem. 2018;32:e4524.
- [22] Ahmadian M, Anbia M. Oxidative desulfurization of liquid fuels using polyoxometalate-based catalysts: A review. Energy Fuels. 2021;35:10347–73.
- [23] Rezvani MA, Imani A. Ultra-deep oxidative desulfurization of real fuels by sandwich-type polyoxometalate immobilized on copper ferrite nanoparticles, Fe₆W₁₈O₇₀ ⊂ CuFe₂O₄, as an efficient heterogeneous nanocatalyst. J Environ Chem Eng. 2021;9:105009.
- [24] Salmanzadeh Otaghsaraei S, Kazemeini M, Hasannia S, Ekramipooya A. Deep oxidative desulfurization via rGO-immobilized tin oxide nanocatalyst: Experimental and theoretical perspectives. Adv Powder Technol. 2022;33:103499.
- [25] Zhai C, Zhu M, Jiang L, Yang T, Zhao Q, Luo Y, et al. Fast triethylamine gas sensing response properties of nanosheets assembled WO₃ hollow microspheres. Appl Surf Sci. 2019:463:1078–84.
- [26] Zuo P, Liu Y, Jiao J, Ren J, Wang R, Jiao W. Ultrafine W₂c well-dispersed on N-doped graphene: extraordinary catalyst for ultrafast oxidative desulfurization of high sulfur liquid fuels. SSRN Electron J. 2022;643:118791.
- [27] Munir M, Saeed M, Ahmad M, Waseem A, Alsaady M, Asif S, et al. Cleaner production of biodiesel from novel non-edible seed oil (Carthamus lanatus L.) via highly reactive and recyclable green nano CoWO3@rGO composite in context of green energy adaptation. Fuel. 2023;332:126265.
- [28] Alam SN, Sharma N, Kumar L. Synthesis of graphene oxide (GO) by modified hummers method and its thermal reduction to obtain reduced graphene oxide (rGO). Graphene. 2017;6:1–18.
- [29] Guex LG, Sacchi B, Peuvot KF, Andersson RL, Pourrahimi AM, Ström V, et al. Experimental review: Chemical reduction of graphene oxide (GO) to reduced graphene oxide (rGO) by aqueous chemistry. Nanoscale. 2017;9:9562–71.

- [30] Li Y, Xiao X, Ye Z. Fabrication of BiVO₄/RGO/Ag₃PO₄ ternary composite photocatalysts with enhanced photocatalytic performance. Appl Surf Sci. 2019;467–468:902–11.
- [31] Zhang W, Li G, Wang W, Qin Y, An T, Xiao X, et al. Enhanced photocatalytic mechanism of Ag₃PO₄ nano-sheets using MS2 (M = Mo, W)/rGO hybrids as co-catalysts for 4-nitrophenol degradation in water. Appl Catal, B. 2018;232:11–8.
- [32] Sharma V, Jain Y, Kumari M, Gupta R, Sharma SK, Sachdev K. Synthesis and characterization of graphene oxide (GO) and reduced graphene oxide (rGO) for gas sensing application. Macromol Symp. 2017;376:1700006.
- [33] Rezvani MA, Maleki Z. Facile synthesis of inorganic-organic Fe₂W₁₈Fe₄@NiO@CTS hybrid nanocatalyst induced efficient performance in oxidative desulfurization of real fuel. Appl Organomet Chem. 2019;33:e4895.
- [34] Kayedi N, Samimi A, Asgari Bajgirani M, Bozorgian A. Enhanced oxidative desulfurization of model fuel: A comprehensive experimental study. S Afr J Chem Eng. 2021;35:153–8.
- [35] Rezvani MA, Khandan S. Synthesis and characterization of new sandwich-type polyoxometalate/nanoceramic nanocomposite, Fe₂W₁₈Fe₄@FeTiO₃, as a highly efficient heterogeneous nanocatalyst for desulfurization of fuel. Solid State Sci. 2019;98:106036.
- [36] Saeed M, Munir M, Nafees M, Shah SSA, Ullah H, Waseem A. Synthesis, characterization and applications of silylation based grafted bentonites for the removal of Sudan dyes: Isothermal, kinetic and thermodynamic studies. Microporous Mesoporous Mater. 2020;291:109697.
- [37] Tariq S, Saeed M, Zahid U, Munir M, Intisar A, Asad Riaz M, et al. Green and eco-friendly adsorption of dyes with organoclay: iso-thermal, kinetic and thermodynamic studies. Toxin Rev. 2022;41:1105–14.
- [38] Rezvani MA, Hadi M, Mirsadri SA. Synthesis of new nanocomposite based on nanoceramic and mono substituted polyoxometalate, PMo₁₁Cd@MnFe₂O₄, with superior catalytic activity for oxidative desulfurization of real fuel. Appl Organomet Chem. 2020;34:e5882.
- [39] Zhang H, Zhang Q, Zhang L, Pei T, Dong L, Zhou P, et al. Acidic polymeric ionic liquids based reduced graphene oxide: An efficient and rewriteable catalyst for oxidative desulfurization. Chem Eng J. 2018;334:285–95.
- [40] Zhao R, Li X, Su J, Gao X. Preparation of WO₃/g-C₃N₄ composites and their application in oxidative desulfurization. Appl Surf Sci. 2017;392:810–6.
- [41] Hasannia S, Kazemeini M, Rashidi A, Seif A. The oxidative desulfurization process performed upon a model fuel utilizing modified molybdenum based nanocatalysts: Experimental and density functional theory investigations under optimally prepared and operated conditions. Appl Surf Sci. 2020;527:146798.
- [42] Chen K, Zhang XM, Yang XF, Jiao MG, Zhou Z, Zhang MH, et al. Electronic structure of heterojunction MoO₂/g-C₃N₄ catalyst for oxidative desulfurization. Appl Catal, B. 2018;238:263–73.